

Reaction mechanism of metal and pyrite under high-pressure and high-temperature conditions and improvement of the properties

Yao Wang(王遥), Dan Xu(徐丹), Shan Gao(高姗), Qi Chen(陈启), Dayi Zhou(周大义), Xin Fan(范鑫), Xin-Jian Li(李欣健), Lijie Chang(常立杰),Yuewen Zhang(张跃文), Hongan Ma(马红安), and Xiao-Peng Jia(贾晓鹏)
Citation: Chin. Phys. B, 2022, 31 (**6**): 066206. DOI: 10.1088/1674-1056/ac4a72
Journal homepage: http://cpb.iphy.ac.cn; http://iopscience.iop.org/cpb

What follows is a list of articles you may be interested in

Bandgap evolution of Mg_3N_2 under pressure: Experimental and theoretical studies

Gang Wu(吴刚), Lu Wang(王璐), Kuo Bao(包括), Xianli Li(李贤丽), Sheng Wang(王升), and Chunhong Xu(徐春红)
Chin. Phys. B, 2022, 31 (**6**): 066205. DOI: 10.1088/1674-1056/ac4cbe

Structural and electrical transport properties of charge density wave material $LaAgSb_2$ under high pressure

Bowen Zhang(张博文), Chao An(安超), Xuliang Chen(陈绪亮), Ying Zhou(周颖), Yonghui Zhou(周永惠), Yifang Yuan(袁亦方), Chunhua Chen(陈春华), Lili Zhang(张丽丽), Xiaoping Yang(杨晓萍), and Zhaorong Yang(杨昭荣)
Chin. Phys. B, 2021, 30 (**7**): 076201. DOI: 10.1088/1674-1056/abf643

Utilizing of high-pressure high-temperature synthesis to enhance the thermoelectric properties of $Zn_{0.98}Al_{0.02}O$ with excellent electrical properties

Qi Chen(陈启), Xinjian Li(李欣健), Yao Wang(王遥), Lijie Chang(常立杰), Jian Wang(王健), Yuewen Zhang(张跃文), Hongan Ma(马红安), and Xiaopeng Jia(贾晓鹏)
Chin. Phys. B, 2021, 30 (**1**): 016202. DOI: 10.1088/1674-1056/abc4dd

Ab initio study on crystal structure and phase stability of ZrC_2 under high pressure

Yong-Liang Guo(郭永亮), Jun-Hong Wei(韦俊红), Xiao Liu(刘潇), Xue-Zhi Ke(柯学志), and Zhao-Yong Jiao(焦照勇)
Chin. Phys. B, 2021, 30 (**1**): 016101. DOI: 10.1088/1674-1056/abb3e7

Neutron powder diffraction and high-pressure synchrotron x-ray diffraction study of tantalum nitrides

Lei-hao Feng(冯雷豪), Qi-wei Hu(胡启威), Li Lei(雷力), Lei-ming Fang(房雷鸣), Lei Qi(戚磊), Lei-lei Zhang(张雷雷), Mei-fang Pu(蒲梅芳), Zi-li Kou(寇自力), Fang Peng(彭放), Xi-ping Chen(陈喜平), Yuan-hua Xia(夏元华), Yohei Kojima(小岛洋平), Hiroaki Ohfuji(大藤宏明), Duan-wei He(贺端威), Bo Chen(陈波), Tetsuo Irifune(入舩徹男)
Chin. Phys. B, 2018, 27 (**2**): 026201. DOI: 10.1088/1674-1056/27/2/026201

Reaction mechanism of metal and pyrite under high-pressure and high-temperature conditions and improvement of the properties

Yao Wang(王遥)[1], Dan Xu(徐丹)[1], Shan Gao(高姗)[1], Qi Chen(陈启)[1], Dayi Zhou(周大义)[1], Xin Fan(范鑫)[1], Xin-Jian Li(李欣健)[1], Lijie Chang(常立杰)[1], Yuewen Zhang(张跃文)[2,†], Hongan Ma(马红安)[1,‡], and Xiao-Peng Jia(贾晓鹏)[1,2]

[1] *State Key Laboratory of Superhard Materials, College of Physics, Jilin University, Changchun* 130012, *China*

[2] *Key Laboratory of Material Physics of Ministry of Education, School of Physics and Microeletronics, Zhengzhou University, Zhengzhou* 450052, *China*

(Received 22 November 2021; revised manuscript received 3 January 2022; accepted manuscript online 12 January 2022)

Pyrite tailings are the main cause of acid mine wastewater. We propose an idea to more effectively use pyrite, and it is modified by exploiting the reducibility of metal represented by Al under high-pressure and high-temperature (HPHT) conditions. Upon increasing the Al addition, the conductivity of pyrite is effectively improved, which is nearly 734 times higher than that of unmodified pyrite at room temperature. First-principles calculations are used to determine the influence of a high pressure on the pyrite lattice. The high pressure increases the thermal stability of pyrite, reduces pyrite to high-conductivity Fe_7S_8 (pyrrhotite) by Al. Through hardness and density tests the influence of Al addition on the hardness and toughness of samples is explored. Finally we discuss the possibility of using other metal-reducing agents to improve the properties of pyrite.

Keywords: high-pressure and high-temperature (HPHT), pyrite, thermoelectric properties, waste recycling

PACS: 62.50.–p, 72.15.Jf, 72.20.–i **DOI:** 10.1088/1674-1056/ac4a72

1. Introduction

The development of human society relies heavily on fossil fuels. However, their effective utilization rate of energy is only 15%–30% and the rest energy is lost in the form of waste heat.[1] Moreover, fossil fuels are non-renewable resources, and their combustion and exploitation have led to severe environmental pollution. Therefore, there is a demand for efficient and clean energy sources. Thermoelectric materials can directly realize the interconversion between thermal energy and electrical energy and can recover waste heat and obtain clean energy.[2–5] At present, two main factors limit the use of thermoelectric materials. One is their cost because conventional thermoelectric materials are often rich in rare elements such as Ag, Sb, Co, Ge, and Te.[6–10] The other is their thermoelectric properties because the dimensionless ZT value is used to measure the performance of thermoelectric materials. $ZT = S^2\sigma T/\kappa$ (σ is the conductivity, S is the Seebeck coefficient, κ is the thermal conductivity, and $S^2\sigma$ is the power factor (PF)).[11] Therefore, improving the performance of cheap thermoelectric materials has become an important research direction for thermoelectric materials.

Pyrite is the cheapest thermoelectric material, while natural pyrite has poor thermoelectric properties (only 10^6), high brittleness, and poor machinability.[12] Pyrite, which is often associated with gold, quartz, iron ore, and coal, is the main sulfur-containing pollutant in fossil fuels.[13–15] With the exploitation of various minerals, many pyrite tailings are abandoned every year, which heavily pollute land and water. Methods to control this pollution have become a hot research topic.[16–19] In recent years, applications of pyrite in different fields have been widely studied, and more effective utilization of pyrite can prevent pollution and reduce resource usage.[20–27] Waste slag can be used as a thermoelectric material to recover large amounts of waste heat generated during the combustion and smelting of fossil fuels. This is of great significance for saving resources, reducing pollutant emissions, and improving energy utilization.

At present, the methods to improve the properties of pyrite are mainly based on synthetic pyrite. The highest ZT value of pyrite materials is only 10^3. For example, the rare elements Co, Se, or Te are added during synthesis to completely replace Fe or S in the crystal lattice to form a solid solution.[28,29] Nanoscale pyrite prepared by high-energy ball milling can be annealed under vacuum conditions to generate high-conductivity Fe_7S_8 impurities that improve pyrite's thermoelectric performance.[30] Fe_7S_8 (pyrrhotite) has a high conductivity.[31] However, the cost to synthesize artificial pyrite is very high, and there are no effective means to modify natural pyrite.

Because aluminum is strongly reducing, the aluminothermic reaction can be used to reduce metal oxides (including iron) into simple metals. In this study, solid solution Al_2S_3 and highly conductive Fe_7S_8 phases are introduced into pyrite by exploiting the reducibility of Al, which can significantly

†Corresponding author. E-mail: zhangyw@zzu.edu.cn
‡Corresponding author. E-mail: maha@jlu.edu.cn

© 2022 Chinese Physical Society and IOP Publishing Ltd

improve the thermoelectric properties of pyrite. The lattice energy of pyrite is increased at a high pressure, which improves its stability and ensures that pyrite is only reduced to Fe_7S_8 instead of Fe. At the same time, another product, Al_2S_3, is dissolved in the sample, which provides more electron carriers.

Using cheap metal Al to improve the properties of pyrite, HPHT is a new route to efficiently utilize natural pyrite and related materials. Based on the modification of pyrite with cheap metals, we propose a new idea for using waste slag as a thermoelectric material to recover waste heat to prevent and control pollution caused by waste slag and to utilize energy more efficiently. Figure 1 explains this process. After ore such as coal is refined, it is concentrated for power generation, and pyrite-rich smelting and tailings are obtained. The modified waste ores with improved thermoelectric properties are assembled into thermoelectric batteries that recover waste heat.

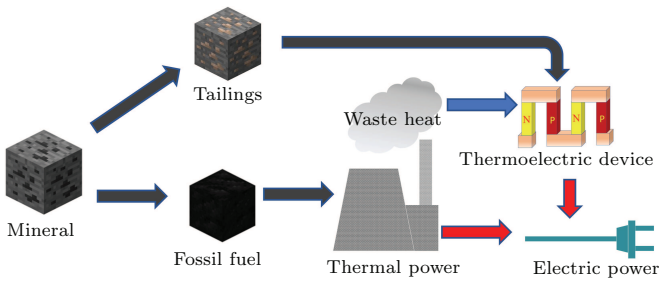


Fig. 1. Waste heat recovery.

2. Experimental and measurement

Natural pyrite (LOT 33199200) was purchased from Strem Chemicals, and aluminum powder (99.9%, lots of #D1719147) and Bi (99.99%, lots of #E1520054) were purchased from Aladdin Company. Pb (99.9%, #51013460) was purchased from Sinopharm Chemical Reagent Co. LTD. They were weighed according to the stoichiometry in Table 1. The weighed samples were evenly mixed in an argon atmosphere and then cold-pressed into cylinders (bottom diameter = 10.5 mm, height = 8 mm). The cylinder was placed in a pyrophyllite assembly, which was assembled and placed in the synthesis chamber of a hinged hexahedron press. The high-pressure reaction was carried out in the hinged hexahedron press (SPD-6 × 1200) in a high-pressure device. The specific assembly is shown in Fig. 2. A platinum–rhodium thermocouple was used to calibrate the temperature of the synthesis chamber, and the electromotive force of the thermocouple changed regularly with the chamber temperature. Using the pressure phase transition point of the standard pressure substance, the corresponding relationship between the oil pressure and cavity pressure was obtained, and the pressure was calibrated. In this paper, the synthesis conditions were 3 GPa, 870 K, and 1 h. During the reaction, the cylinder was wrapped in molybdenum with a high melting point to prevent the sample from being polluted. After obtaining a block sample, to make the samples more uniform, the bulk samples were crushed, ground, and then sintered for another 30 min at 3 GPa and 870 K.

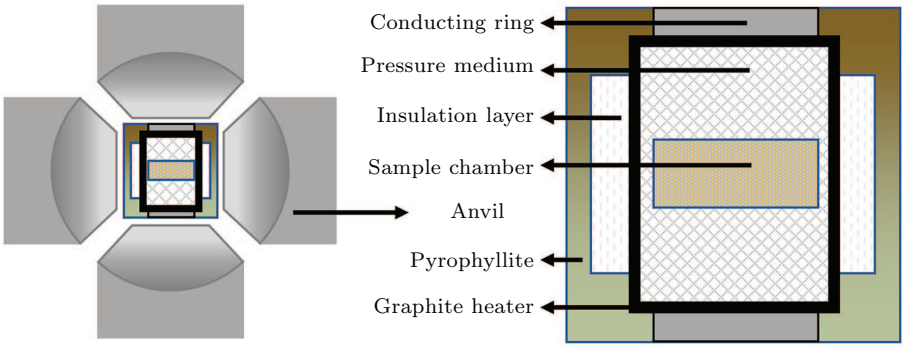


Fig. 2. Assembly diagram.

Table 1. Experimental samples and conditions.

No.	Al:FeS_2 (mole ratio)	Temperature (K)	Pressure (GPa)
1	0:1	870	3
2	0.05:1	870	3
3	0.2:1	870	3
4	0.4:1	870	3
5	0.6:1	870	3
6	0.6:1	870	atmospheric pressure
7	$Bi_{0.4}FeS_2$	870	3
8	$Pb_{0.3}FeS_2$	870	3

2.1. Measurements

First-principles calculations were used to simulate and calculate the influence of high pressure on the atomic spacing in the pyrite lattice. X-ray diffraction (XRD, Rigaku D/Max 2550V/PC, Japan Cu $K\alpha$ radiation, $\lambda = 0.15418$ nm) and variable temperature x-ray diffraction (SmartLab SE x-ray diffractometer, Rigaku SmartLab, Japan Cu $K\alpha$ radiation) were used to characterize the synthesized samples. The micromorphology and structure of the samples were observed by using a field emission scanning electron microscope (SEM, Magel-

lan 400). The valence states of elements in the samples were measured by XPS (Thermo Scientific Escalab 250Xi). The phase composition of the samples was analyzed by a metallographic microscope (SOPTOP CX40M). Cutting the block sample into strips of 3 mm×3 mm×8 mm, the electrical conductivity and Seebeck coefficient of samples from 320–570 K were measured by a Joule Yacht/Namicro-3l thermoelectric measurement system. Samples with the same properties were processed into disks, and the thermal diffusion coefficients of samples at temperatures between 320 K and 870 K were measured by laser thermal conductivity instrument LFA-467 (Germany, Netzsch) using the laser flash method. The heat capacity C_p of samples was calculated by the Dulong–Petit law, and the density ρ of samples was measured by Archimedes' principle using an AE124J electronic balance. According to the formula ($\kappa = \lambda C_p D$), the thermal conductivity of the sample was calculated. Vickers Indenter HV-5IS was used to measure the mechanical hardness of the samples.

3. Results and discussion

3.1. HPHT reaction

HPHT can change the properties of materials and increase the reaction efficiency.[32,33] The structure of pyrite is similar to that of NaCl, and its thermal stability is easily affected by pressure.[34,35] According to first-principles calculations, changes in the atomic spacing of pyrite under different pressures were simulated and calculated in Table 2. According to changes in the atomic spacing and Born–Landé formula, $U = KAZ_1Z_2(1-1/n)/R_0$, the variations in the lattice energy of pyrite with pressure were calculated. U is the lattice energy, R_0 is the interatomic spacing, Z_1 and Z_2 are the absolute values of positive- and negative-charged ions, and K, A, and n are constants. The changing trends in the lattice energy of the same substance under a high pressure are the same as that of $1/R_0$. Under a high pressure, the distance between ions in pyrite decreases due to compression, and the lattice energy increases accordingly. The lattice energy of pyrite shows the most obvious increase between 0–3 GPa (Fig. 3(a)). The improvement in the thermal stability of pyrite under a high pressure is a macroscopic manifestation of the increasing lattice energy. Therefore, the related diffraction peak of the FeS_2 thermal decomposition product is not observed in the XRD pattern of sample 1 (Al 0) at 3 GPa (Fig. 4). Pyrite will decompose at 870 K under normal pressure.[30,36]

Table 2. Variation in the atomic spacing with pressure.

Pressure (GPa)	Fe–S (Å)	S–S (Å)
	2.25973	2.19941
3	2.23220	2.17569
6	2.22203	2.17033
9	2.21098	2.16159
12	2.20204	2.15226

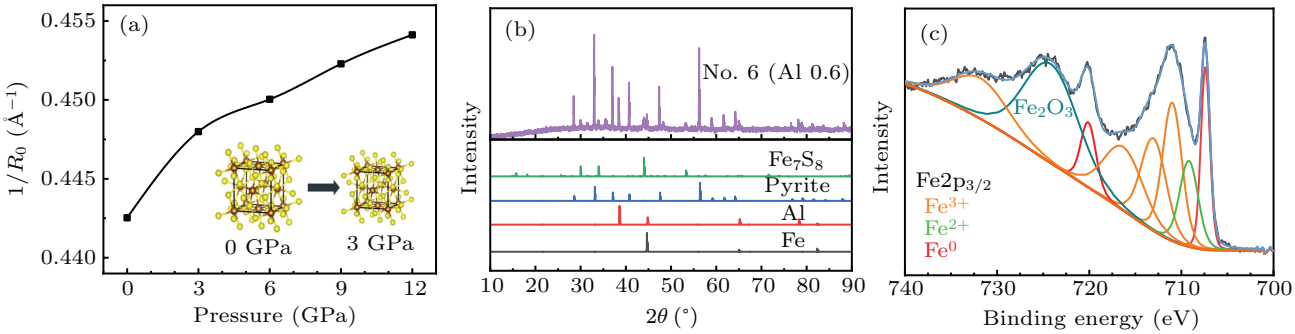


Fig. 3. (a) Changes in the $1/R_0$ with pressure (pyrite). (b) The XRD patterns of sample 6. (C) The Fe $2p_{3/2}$ XPS spectra of sample 6.

Changes in the lattice energy can affect the reaction between pyrite and aluminum. Diffraction peaks of aluminum and iron were observed in the XRD patterns of sample 6 (obtained at atmospheric pressure, Fig. 3(b)) in the XRD patterns of sample 5 (Fig. 4). We used XPS test to supplement the XRD test results, and found Fe^0, Fe^{2+}, Fe^{3+} signal in the test results of sample 6.[37–39] Natural pyrite was used in this experiment, and its composition is relatively complex. If the Fe in sample 6 was completely produced by aluminum reduction of pyrite, pyrite would be reduced to elemental Fe by aluminum under a normal pressure, but not at a high pressure. Pyrite, with a higher lattice energy under high pressure, can only be reduced to Fe_7S_8.

The XRD patterns show the changes in the sample composition after aluminum addition under a high pressure (Fig. 4). The XRD peak intensity of Fe_7S_8 in samples increased with increasing the Al addition. The amounts of Al_2S_3 and Fe_7S_8 in sample 2 (Al 0.05) were small, which did not reach the solid solubility limit. No diffraction peaks related to Al_2S_3 and Fe_7S_8 were found in the XRD pattern. Upon increasing the Al addition, the lattice spacing of the sample increased, and the XRD peak position of the sample shifted to a lower angle. A very weak diffraction peak of Al_2S_3 appeared in the pattern of sample 3 (Al 0.2), indicating that Al_2S_3 reached the solid solution limit.

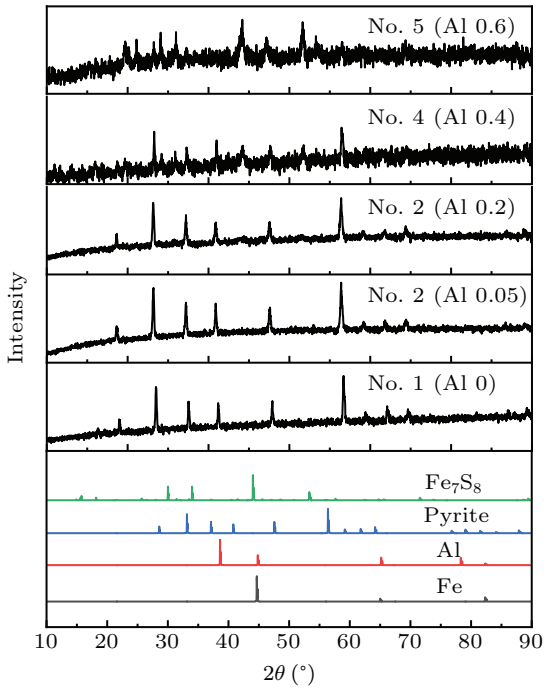


Fig. 4. The XRD patterns for the HPHT reaction with different amounts of Al added.

3.2. Microstructures

Changes in the microstructure of pyrite after modification can affect its thermal conductivity.[40,41] The SEM images show the cross-sectional micromorphology of the sample (Fig. 5). Upon increasing the Al concentration, the material's grain structure tended to become flaky. The grains of sample 1 (Al 0) were clustered and tightly stacked together (Figs. 5(a) and 5(b)). The SEM image of sample 2 (Al 0.05) shows that a large number of flaky grains appeared in the samples, and the grain size was refined, even though the amount of Al added was low (Figs. 5(c) and 5(d)). Upon further increasing the Al concentration, the granular grains in sample 3 (Al 0.2) were further reduced, the grain arrangement became more regular, and the grains were enlarged and stacked with each other to form obvious layers (Figs. 5(e) and 5(f)). This phenomenon was more obvious in samples 4 (Al 0.4) and 5 (Al 0.6).

The formation of new phases is an important reason for the changes in pyrite's properties. The metallographic microscope photos of the samples show that upon increasing the amount of Al, the composition of other phases in the samples increased (Fig. 6). The gray part is a newly formed phase. The proportion of the new phase in sample 3 (Al 0.2) was relatively small due to the small amount of Al added, but a large amount of the new phase was generated in sample 5 (Al 0.6) with a large amount of Al added.

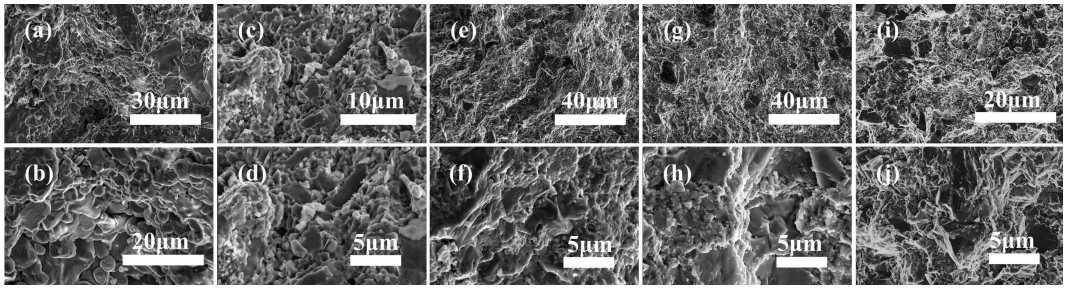


Fig. 5. SEM images of samples with different Al addition amounts [(a), (b)] sample 1 (Al 0), [(c), (d)] sample 2 (Al 0.05), [(e), (f)] sample 3 (Al 0.2), [(g), (h)] sample 4 (Al 0.4), [(i), (j)] sample 5 (Al 0.6).

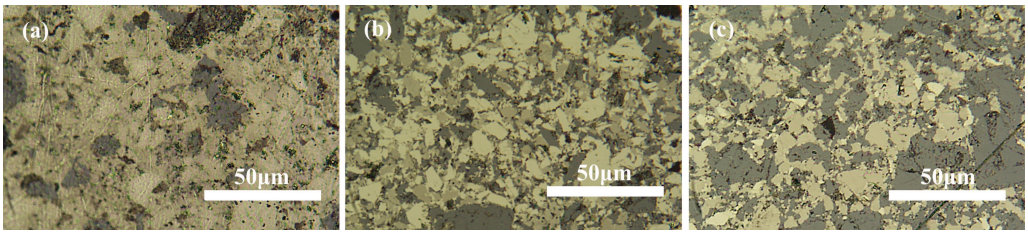


Fig. 6. Metallographic images of samples with different amounts of Al added: (a) sample 3 (Al 0.2), (b) sample 4 (Al 0.4), and (c) sample 5 (Al 0.6).

3.3. Thermoelectric properties

The electrical conductivity of pyrite is extremely low, so improving its electrical conductivity can optimize its thermoelectric properties. The electrical conductivity of sample 1 (Al 0) at room temperature was only 9.89×10^{-2} S/cm (Fig. 7(a)). At 370 K, the conductivity of sample 5 (Al 0.6) increased to 72.58 S/cm, which is about 734-times higher than that of sample 1 (Al 0). At 570 K, the conductivity of sample 5 (Al 0.6) was the highest, which is about 259 times higher than that of sample 1 (Al 0). All samples showed typical semiconductor properties, and the conductivity increased with the temperature.

The Seebeck coefficient of the sample depends on the temperature (Fig. 7(b)). All samples were p-type semiconductors at room temperature, and the Seebeck coefficient was

greater than zero. Upon increasing the temperature, the sample changed from a p-type semiconductor to an n-type semiconductor, and the Seebeck coefficient became negative. The reason for this is that the Seebeck coefficient of a semiconductor is determined by its internal majority carriers. For pyrite materials, the holes (positive charge) were the main carriers at low temperatures. Thus, pyrite is a p-type semiconductor at this time. Upon increasing the temperature, more electrons (negative charge) were gradually excited until their number exceeded the holes. At that time, the semiconductor properties of the samples were fundamentally changed, i.e., from a p-type semiconductor to an n-type semiconductor.[30]

The two reaction products (Al_2S_3 and Fe_7S_8) affecting the properties are synergistic, they both provide more charge carriers for the system. The changes in the conductivity and Seebeck coefficient were mainly due to the new-phase Fe_7S_8 and Al_2S_3 solid solution. Fe_7S_8 has high electrical conductivity [$(1.40 \pm 0.05) \times 10^5$ S/m].[30,31] Al_2S_3 forms a solid solution with Fe_7S_8, which increases the conductivity of the sample, but it does not conduct electricity by itself. Al dopant acts as a donor to produce electrons according to the following expression:[4]

$$4Al + 7FeS_2 \xrightarrow{HPHT} 2Al_2S_3 + Fe_7S_8,$$
$$Al_2S_3 \xrightarrow{Fe_7S_8} 2Al^{\bullet}_{Fe}S_3 + 2e' + 2S^{X}_{S} + S.$$

The rise in temperature helps to increase the concentration of charge carriers in the semiconductor, which changes the electrical properties of the sample, especially in the solid solution. Point defects in semiconductors are an important source of carriers. With the temperature increasing, the point defect concentration will increase according to the equation[4]

$$C = N \exp\left(-\frac{E^{f}}{k_B T}\right),$$

where C is the point defect concentration, N is the number of sites available for defect formation, E^f is the defect formation energy, k_B is the Boltzmann's constant, and T is the temperature. With the temperature increasing, the concentration of point defect will rise and the electrical properties change. Therefore, with the increasing Al addition and temperature, the electrical properties of the samples change dramatically.

In experiment, less Fe_7S_8 was produced in sample 2 (Al 0.05), and the sample properties were mainly affected by the solid solution of Al_2S_3. The formation of a solid solution provided more electrons for the samples. Therefore, sample 2 (Al 0.05) was transformed into an n-type semiconductor from 320 K to 370 K. The Al_2S_3 in sample 3 (Al 0.2) reached the solid solubility limit, and Fe_7S_8 became the main factor affecting the properties of the sample. Fe_7S_8 provided more holes for the sample, so the temperature of the sample transformed into an n-type semiconductor between 420 K and 470 K. At 570 K, all samples were converted into n-type semiconductors, and the Seebeck coefficient decreased upon increasing the aluminum addition.

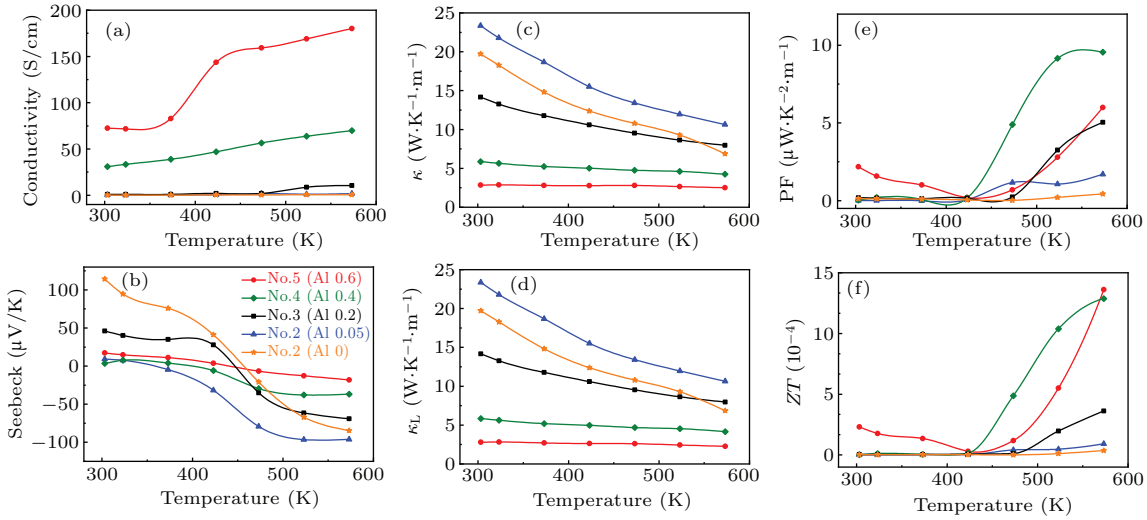


Fig. 7. Changes in the electrical conductivity, Seebeck coefficient, thermal conductivity, lattice thermal conductivity, and power factor of samples with temperature.

The total thermal conductivity was determined from the electronic thermal conductivity and lattice thermal conductivity. The sample's thermal conductivity ($W \cdot K^{-1} \cdot m^{-1}$) changed regularly upon changing the test temperature and Al addition (Figs. 7(c) and 7(d)). The thermal conductivity of pyrite is very high, and as the temperature increased from 300 K to 570 K, the thermal conductivity of sample 1 (Al 0) decreased from 19.7 $W \cdot K^{-1} \cdot m^{-1}$ to 6.8 $W \cdot K^{-1} \cdot m^{-1}$. The thermal conductivity of sample 2 (Al 0.05) with a small amount of Al decreased from 23.3 $W \cdot K^{-1} \cdot m^{-1}$ to 10.6 $W \cdot K^{-1} \cdot m^{-1}$. Upon increasing the Al addition ratio, the thermal conductivity of the samples decreased significantly. Sample 5 (Al 0.6) had the lowest thermal conductivity, dropping from 2.9 $W \cdot K^{-1} \cdot m^{-1}$ to 2.5 $W \cdot K^{-1} \cdot m^{-1}$ upon increasing the temperature. The de-

crease in the thermal conductivity of samples was related to an increase in the Fe_7S_8 content of samples.[30] In addition, as the sample structure became more complex, the phonon scattering ability increased, which also reduced the thermal conductivity.

According to the conductivity and Seebeck coefficient of the sample, the power factor ($\mu W \cdot K^{-2} \cdot m^{-1}$) of the sample was calculated (Fig. 7(e)). As the sample transformed between n- and p-type semiconductors with temperature, its power factor decreased first and then increased. At 573 K, all samples obtained the highest power factor, among which sample 4 (Al 0.4) had the highest power factor (PF = 9.55 $\mu W \cdot K^{-2} \cdot m^{-1}$).

According to the power factor (PF) and thermal conductivity (σ), the dimensionless quality factor (ZT) of the sample was calculated (Fig. 7(f)). The ZT value of sample 1 (Al 0) without added Al was only 1.99×10^{-6} at 370 K, and only 3.6×10^{-5} at 570 K. After modification, the power factor of the sample increased, and the thermal conductivity decreased. The thermoelectric properties of sample 5 (Al 0.6) were better than those of other samples, and the ZT value at 300 K was 2.3×10^{-4}. The ZT reached a peak value of 1.36×10^{3} at 570 K, which is nearly 38 times higher than that of sample 1 (Al 0) at the same temperature. The increase in the ZT value indicates that adding Al under HPHT conditions improved the thermoelectric properties of pyrite.

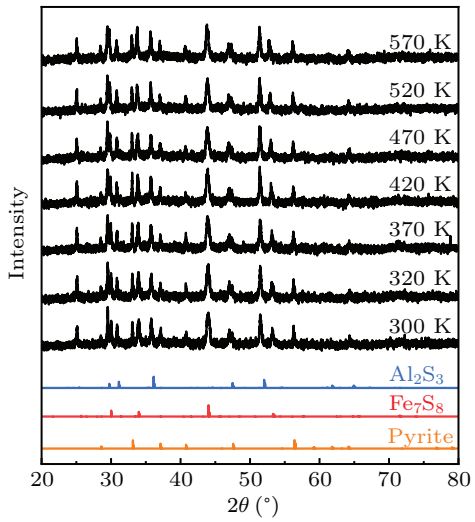


Fig. 8. Variable temperature XRD patterns of sample 6 (300–570 K).

In order to study the changes of structure and composition of the sample during the heating process, we carried out variational temperature XRD tests on sample 5 (Al 0.6). The XRD peaks of the samples shift slightly to a small angle with the increase of temperature, and there is no obvious change. This slight deviation is due to thermal expansion of the lattice. This suggests that with the increase of temperature, the phase composition of the sample does not change significantly. In the test temperature range, the sample is stable without decomposition or phase transformation. Therefore, the increase of electrical properties with temperature is not due to phase transition or new reactions.

3.4. Mechanical properties

Pyrite is a brittle material with poor machinability, and aluminum is often used as a toughening agent for brittle materials to reduce their hardness. After polishing the samples, random positions on each sample were selected, and a load of 500 g was applied for 10 s to make impressions with different areas (Fig. 9). Changes in the indentation indicate changes in the hardness of the sample. Sample 1 (Al 0) has the smallest indentation area, and cracks with a length of about 30 μm appeared around it. The cracks near the indentation mean that the fracture toughness of the sample was relatively poor. However, with increasing the Al addition, the indentation area increased, and there was no fracture. The increase in the indentation area indicates a decrease in the sample hardness, while the disappearance of cracks near it indicates that the fracture toughness of the sample increased. The hardness of the sample was calculated by the indentation area, and an average value was obtained. The change in the hardness and density of the sample with the Al addition amount is shown in Fig. 10. Upon increasing the aluminum content, the hardness of the samples gradually decreased from an initial value of 10.01 GPa to 4.09 GPa. At the same time, the density of the sample gradually decreased from 4.78 g/cm^3 to 3.74 g/cm^3. The increase in the fracture toughness and the decrease in the hardness and density indicate that the samples were more difficult to fracture, less difficult to process, and lighter for practical applications.

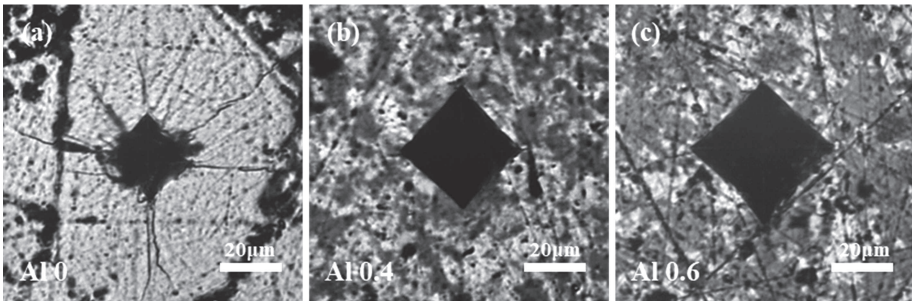


Fig. 9. Indentations of different samples under the same load.

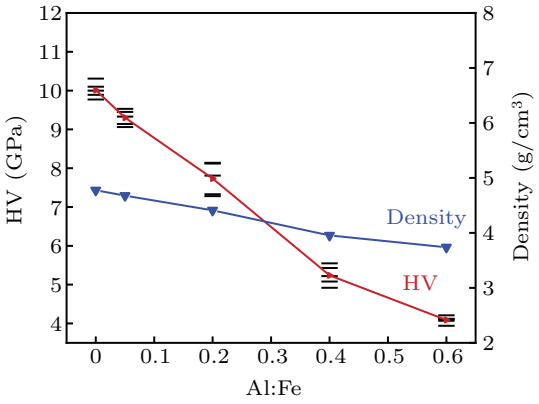


Fig. 10. Changes in the Vickers hardness and densities of samples with different additive concentrations.

Under the same HPHT conditions as above, as Al_2S_3 is formed after reduction of Al, galena and bismuthinite are formed after absorption of sulfur in pyrite by the two metals, see Fig. 11(d). After the reaction, the conductivity, Seebeck coefficient and power factor of the sample improved, see Figs. 11(a), 11(b), and 11(c). This improvement is partly the formation of highly conductive phases due to the loss of sulfur in pyrite. On the other hand, galena and bismuthinite, unlike Al_2S_3, are themselves thermoelectric materials worthy of further optimization. The formation of galena and bismuthinite further increases the room for improvement of material properties. It is foreseeable that improving the properties of metal sulfides can further improve the overall properties of the material.

With the expansion of the selection range of metal-reducing agents, the room for improvement of pyrite properties becomes larger. For example, multiple metal reducing agents can work together. The principle can be used as an intermediate process to optimize pyrite and related materials or pyrite as a dopant to add magnetic components (pyrrhotite) to other thermoelectric materials. Therefore, this result is worthy of further study as a supplement to previous work on modification of pyrite and related materials.

The use of high pressure can form many lattice defects, and high-pressure quenching promoted the growth of nanoscale grains. The defects improved the thermoelectric properties of the material, suggesting that HPHT can be used to obtain desired morphologies.[34]

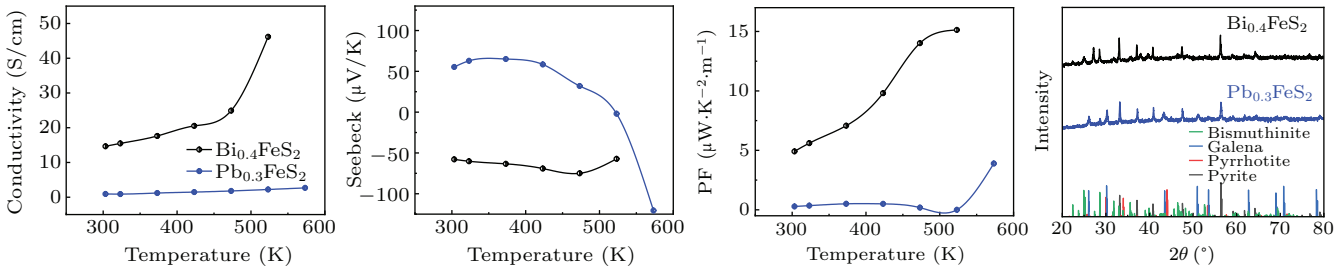


Fig. 11. Changes in the electrical conductivity (a), Seebeck coefficient (b), and power factor (c) of samples ($Bi_{0.4}FeS_2$,$Pb_{0.3}FeS_2$) with temperature. (d) The XRD patterns.

4. Conclusion

The reducibility of aluminum under high pressure improves pyrite's electrical conductivity, decreases its thermal conductivity, and significantly enhances its thermoelectric properties. The high pressure enhances the stability of pyrite, and pyrite could only be reduced to Fe_7S_8 by Al at HPHT. Therefore, the conductivity of the sample at room temperature is increased by about 734 times while maintaining the semiconductor properties of the sample. After modification, the sample composition is more complex, which causes more phonon scattering and decreases the thermal conductivity. Compared with the sample without Al addition, the ZT value at the same temperature is about 38 times higher than that before modification. The addition of aluminum changes the mechanical properties of the samples. The hardness and density of the sample are reduced, the fracture toughness of the sample is improved, and the machinability of the sample is increased. Based on the modification of pyrite with cheap metals, a new idea of using waste slag as a thermoelectric material to recover waste heat is proposed. The experimental results can also be extended to other elements (Bi, Pb, etc.) based on Al, greatly expanding the optimization space of material properties.

Acknowledgements

Project supported by the National Natural Science Foundation of China (Grant No. 51171070), the Project of Jilin Science and Technology Development Plan (Grant No. 20170101045JC), the Natural Science Foundation of Chongqing, China (Grant No. cstc2019jcyj-msxmX0391), and the Science and Technology Research Program of Chongqing Municipal Education Commission (Grant No. KJQN201901405).

References

[1] Farnoosh A, Lantz F and Percebois J 2014 *Energy* **69** 299
[2] Bel L E 2008 *Science* **321** 1457
[3] Shi X L, Zou J and Chen Z G 2020 *Chem. Rev.* **120** 7399
[4] Chen Q, Li X, Wang Y, Chang L, Wang J, Zhang Y, Ma H and Jia X 2021 *Chin. Phys. B* **30** 016202
[5] Ji W, Shi X L, Liu W D, Yuan H, Zheng K, Wan B, Shen W, Zhang Z, Fang C, Wang Q, Chen L, Zhang Y, Jia X and Chen Z G 2021 *Nano Energy* **87** 106171

[6] Zhang Y, Jia X, Sun H, Sun B, Liu B, Liu H, Kong L and Ma H 2016 *RSC Adv.* **6** 7378

[7] Su T, Zhu P, Ma H, Ren G, Chen L, Guo W, Iami Y and Jia X 2006 *Solid State Commun.* **138** 580

[8] Zhang Y, Ma H, Sun B, Liu B, Liu H, Kong L, Liu B, Jia X and Chen X 2017 *J. Alloys Compd.* **715** 344

[9] Deng L, Jia X P, Su T C, Jiang Y P, Zheng S Z, Guo X and Ma H A 2011 *Mater. Lett.* **65** 1582

[10] Liu B W, Ma H G, Huo D X, Liu H Q, Liu B M, Chen J X and Jia X P 2018 *J. Materiom.* **4** 68

[11] Beekman M, Morelli D T and Nolas G S 2016 *Nat. Mater* **15** 11

[12] Zuniga-Puelles E, Cardoso-Gil R, Bobnar M, Veremchuk I, Himcinschi C, Hennig C, Kortus J, Heidee G and Gumeniuk R 2019 *Dalton Trans.* **48** 10703

[13] Luo M, Zhou L, Kuang C, Wang C and Zhang H 2021 *Fuel* **285** 119213

[14] Forson P, Skinner W and Asamoah R 2021 *Powder Technol.* **385** 12

[15] Rieder M, Crelling J C, Sustai O, Drabek M, Weiss Z and Klementova M 2007 *Int. J. Coal Geol.* **71** 115

[16] Fortes J C, Sarmiento A M, Luis A T, Santisteban M, Davila J M, Cordoba F and Grande J A 2021 *Water Air Soil Pollut.* **232** 88

[17] Garcia-Carmona M, Garcia-Robles H, Torrano C T, Ondono E F, Moreno J L, Aragon M S and Peinado F J M 2019 *Sci. Total Environ.* **650** 933

[18] Grande J A, Santisteban M, Perez-Ostale E, Valente T, de la Torre M L, Gomes P and Barrios-Parra F 2018 *Mine Water Environ.* **37** 211

[19] Grande J A, Santisteban M, de la Torre M L, Valente T and Perez-Ostale E 2013 *Mine Water Environ.* **32** 321

[20] Morales-Gallardo M V, Ayala A M, Pal M, Cortes Jacome M A, Toledo Antonio J A and Mathews N R 2016 *Chem. Phys. Lett.* **660** 93

[21] Yuan B, Luan W and Tu S T 2015 *Mater. Lett.* **142** 160

[22] Zou J, Zhao J, Wang B, Chen S, Chen P, Ran Q, Li L, Wang X, Yao J, Li H, Huang J, Niu X and Wang L 2020 *ACS Appl. Mater. Interfaces* **12** 44850

[23] Venkateshalu S, Kumar P G, Kollu P, Jeong S K and Gracea A N 2018 *Electrochim. Acta* **290** 378

[24] Faber M S, Lukowski M A, Ding Q, Kaiser N S and Jin S 2014 *J. Phys. Chem. C* **118** 21347

[25] Wang F M, Li Y C, Shifa T A, Liu K L, Wang F, Wang Z X, Xu P, Wang Q S and He J 2016 *Angew. Chem.-Int. Ed.* **55** 6919

[26] Gao M R, Zheng Y R, Jiang J and Yu S H 2017 *Account. Chem. Res.* **50** 2194

[27] Pandey P, Gahlawat S and Ingole P P 2020 *ACS Sustain. Chem. Eng.* **8** 15584

[28] Clamagirand J M, Ares J R, Flores E, Diaz-Chao P, Leardini F, Ferrer I J and Sanchez C 2016 *Thin Solid Films* **600** 19

[29] Gudelli V K, Kanchana V, Vaitheeswaran G, Valsakumar M C and Mahanti S D 2014 *RSC Adv.* **4** 9424

[30] Wang C, Niu Y, Jiang J, Chen Y D, Tian H Q, Zhang R, Zhou T, Xia J F, Pan Y and Wang S Y 2018 *Nano Energy* **45** 432

[31] Worm H U, Clark D and Dekkers M J 1993 *Geophys. J. Int.* **114** 127

[32] Li Y D, Cheng Y S, Su M J, Ran Q F, Wang C X, Ma H A, Fang C and Chen L C 2019 *Chin. Phys. B* **29** 078101

[33] Fang S, Ma H A, Guo L S, ChenL C, Wang Y, Ding L Y, Cai Z H, Wang J and Jia X P 2019 *Chin. Phys. B* **28** 098101

[34] Lu Z Y and Li J 2015 *Am. Miner* **100** 1892

[35] Gudelli V K, Kanchana V, Appalakondaiah S, Vaitheeswaran G and Valsakumar M C 2013 *J. Phys. Chem. C* **117** 21120

[36] Labus M 2021 *Fuel* **287** 119529

[37] Natalia Chubar, Vasyl Gerda, Małgorzata Szlachta, Ganna Yablokova 2021 *Solid State Sci.* **121** 106752

[38] Idczak K and Idczak R 2020 *Metall. Mater. Trans. Part A* **51** 3076

[39] Yamashita T and Hayes P 2007 *Appl. Surf. Sci.* **254** 2441

[40] Li X J, Chang L J, Chen Q, Wang Y, Wang C X, Wang J, Zhang Y W, Ma H A and Jia X P 2021 *Ceram. Int.* **47** 17627

[41] Ji G Y, Chang L J, Ma H A, Liu B M, Chen Q, Wang Y, Li X J, Wang J N, Zhang Y W and Jia X P 2021 *J. Alloys Compd.* **850** 156623